Bulletin of the Earthquake
Research Institute
Vol. 46 (1968), pp. 1237-1268

60. *A Long Wave in the Vicinity of an Estuary* [V].

By Takao Momoi,

Earthquake Research Institute.

(Read Sept. 17, 1968.—Received Sept. 30, 1968.)

Abstract

In this report, the variations of the amplitude and phase of RST (resultant) and RD (reflected and diffracted) waves and further the decaying modes in the canal are discussed through the numerical calculation. The following facts are then exposed.

The same behavior of the wave as that in the case of the breakwater (*Momoi*, 1967), i.e., the appearance of high waves (>2.0 in amplitude) and rotating waves is found for RST wave in the open sea.

Concerning the decaying modes in the canal which show the reflecting behavior of the wave in the canal, it is found that the invading wave advances along the (two) banks of the canal to be reflected toward the open sea in the middle part.

In Section 6, the behavior of the wave around the estuary is elucidated through the numerical calculation of the wave around the right-angled corner.

In the last section, the examination of the wave around the estuary is made by use of the approximated method (of mirror image) using the model of the right-angled corner.

1. Introduction

Succeeding the previous works (*Momoi*, 1965a, 1965b, 1966 and 1968), the long wave around the estuary is discussed in this paper. The last article is referred to as paper IV in the following sections.

2. Theory

The definitions and notations used in the present paper are exactly the same as those in the previous works, unless otherwise stated.

In the previous paper IV, we have obtained the following infinite simultaneous equations:

$$i\cdot\frac{k_1^{(m)}d}{kd}\cdot\sum_{n=0}^{\infty}I(J_{2n},m)\bar{\zeta}_2^{(2n)}+\sum_{n=0}^{\infty}I\left(\frac{J_{2n+1}}{r},m\right)\zeta_2^{(2n+1)}=0 \qquad (1)$$

$$(m=0,1,2,\cdots)$$

and

$$\varepsilon_m \bar{\zeta}_2^{(2m)} - ikd \sum_{n=0}^{\infty} \frac{2n+1}{(2n+1)^2-(2m)^2} \cdot \zeta_2^{(2n+1)} \cdot \{J_{2n+1}(kd) H_{2m}^{(1)\prime}(kd) - J'_{2n+1}(kd) H_{2m}^{(1)}(kd)\} = 2\zeta_0 \qquad (2)$$
$$(m=0, 1, 2, \cdots),$$

where

$$\left.\begin{aligned} &\varepsilon_0 = 1 , \qquad \varepsilon_m = 1/2 \qquad (m \geqq 1) , \\ &I(J_{2n}, m) = \int_0^{kd} J_{2n}(x) \cos \frac{m\pi}{kd} x dx , \\ &I\left(\frac{J_{2n+1}}{r}, m\right) = (2n+1) \int_0^{kd} \frac{J_{2n+1}(x)}{x} \cos \frac{m\pi}{kd} x dx , \\ &k_1^{(m)} d = \sqrt{(kd)^2 - (m\pi)^2} . \end{aligned}\right\} \qquad (3)$$

Equations (1) and (2) are given respectively in (6) and (7) of paper IV.

In the foregoing papers, the calculations of integration (3) were carried out through the use of the ascending power series of the Bessel functions $J_m(x)$ which are approximated by finite series in proportion to the extent of the used approximation. In the present work, the direct calculation of integral (3) was made by use of Simpson's formula and Filon's method (*Filon*, 1928). The former is employed in the calculation of integral (3) for $m=0$, while the latter is used in the calculation for $m \geqq 1$. Filon devised a new method which makes possible the numerical calculation of the integral

$$\int_a^b \psi(x) \sin (kx+\varepsilon) dx , \qquad (4)$$

with large k (constant), where $\psi(x)$ is a function with a limited number of turning-points in the range of integration, a and b the lower and upper limits, and ε the phase. The actual calculation of integral (4) by quadrature when k is large is, in practice, a matter of very considerable difficulty on account of the rapid oscillation of the function $\sin(kx+\varepsilon)$ which makes the application of the ordinary quadrature formula such as Simpson's prohibitive.

In the calculation of (3) by Filon's method, setting $J_{2n}(x)$ (or $J_{2n+1}(x)/x$) equal to $\psi(x)$, $m\pi/kd$ $(m \geqq 1)$ to k, 0 to a, and kd to b, integral (3) is reduced to integral (4), where $\varepsilon = \pi/2$. Following the procedure devised by Filon, integral (3) for $m \geqq 1$ can then be calculated.

When the approximation

$$\left.\begin{array}{ll} J_m(x)\fallingdotseq 0 & (m\leqq 2l+1) \\ J_m(x)\equiv 0 & (m>2l+1) \end{array}\right\} \quad \text{for} \quad |x|\leqq kd \tag{5}$$

where $l=1, 2, 3, \cdots$, is given upon *infinite* simultaneous equations (1) and (2), these are reduced to the following *finite* simultaneous equations:

$$i\cdot\frac{k_1^{(m)}d}{kd}\sum_{n=0}^{l} I(J_{2n}, m)\bar{\zeta}_2^{(2n)}+\sum_{n=0}^{l} I\left(\frac{J_{2n+1}}{r}, m\right)\zeta_2^{(2n+1)}=0 \tag{6}$$

$$(m=0, 1, 2, \cdots, l) \qquad \text{(from (1))}$$

and

$$\varepsilon_m\bar{\zeta}_2^{(2m)}-ikd\sum_{n=0}^{l}\frac{2n+1}{(2n+1)^2-(2m)^2}\zeta_2^{(2n+1)} \cdot\{J_{2n+1}(kd)H_{2m}^{(1)\prime}(kd)-J'_{2n+1}(kd)H_{2m}^{(1)}(kd)\}=2\zeta_0 \tag{7}$$

$$(m=0, 1, 2, \cdots, l) \qquad \text{(from (2))}.$$

The above reduction is the second step of our method (the method of the buffer domain) (it is the first step to express the wave height by orthogonal functions).

Solving the above equations (6) and (7), the unknowns

$$\bar{\zeta}_2^{(2n)} \text{ and } \zeta_2^{(2n+1)} \qquad (n=0, 1, 2, \cdots, l) \tag{8}$$

begin to be known.

Under the approximation (5), equations (1) and (3) of paper IV become as follows:

$$\zeta_1^{(m)}=\frac{1}{\varepsilon_m kd}\sum_{n=0}^{l} I(J_{2n}, m)\bar{\zeta}_2^{(2n)} \tag{9}$$

$$(m=0, 1, 2, \cdots) \qquad \text{(from (1) of paper IV)},$$

$$\zeta_3^{(2m)}=\frac{1}{H_{2m}^{(1)}(kd)}\left\{J_{2m}(kd)\left(\bar{\zeta}_2^{(2m)}-\frac{2}{\varepsilon_m}\zeta_0\right)+\frac{1}{\varepsilon_m}\cdot\frac{2}{\pi}\sum_{n=0}^{l}\frac{(2n+1)J_{2n+1}(kd)}{(2n+1)^2-(2m)^2}\zeta_2^{(2n+1)}\right\} \tag{10}$$

$$(m=0, 1, 2, \cdots, l) \qquad \text{(from (3) of paper IV)},$$

and

$$\zeta_3^{(2m)}=\frac{1}{iY_{2m}(kd)}\cdot\frac{4}{\pi}\sum_{n=0}^{l}\frac{(2n+1)J_{2n+1}(kd)}{(2n+1)^2-(2m)^2}\zeta_2^{(2n+1)} \tag{11}$$

$$(m=l+1, l+2, \cdots) \qquad \text{(from (3) of paper IV)}.$$

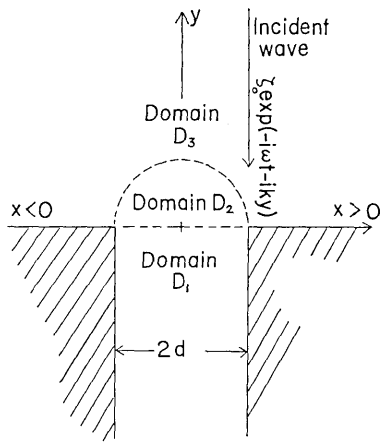

Fig. 1. Geometry of the model used.

Substitution of (8) into (9) to (11) makes possible the calculation of

$$\zeta_1^{(m)} \text{ and } \zeta_3^{(2m)} \quad (m=0, 1, 2, \cdots) . \tag{12}$$

Under the approximation (5), the serial expressions of the wave height in the domains D_1, D_2 and D_3 (refer to Fig. 1) are respectively

$$\zeta_1 = \sum_{m=0}^{\infty} \zeta_1^{(m)} \cos \frac{m\pi}{d} x \cdot \exp\{-ik_1^{(m)} y\} , \tag{13}$$

$$\zeta_2 = \sum_{n=0}^{l} \{\bar{\zeta}_2^{(2n)} \cos 2n\theta J_{2n}(kr) + \zeta_2^{(2n+1)} \sin (2n+1)\theta J_{2n+1}(kr)\} \tag{14}$$

and

$$\zeta_3 = 2\zeta_0 \cos ky + \sum_{m=0}^{\infty} \zeta_3^{(2m)} \cos 2m\theta H_{2m}^{(1)}(kr) . \tag{15}$$

For the derivation of the above expressions, reader should refer to the previous work (*Momoi*, 1965a). Using the factors $\zeta_1^{(m)}$, $\bar{\zeta}_2^{(2n)}$, $\zeta_2^{(2n+1)}$ and $\zeta_3^{(2m)}$ which have been obtained in (8) and (12), the behavior of the wave can be discussed through the expressions (13) to (15).

The above-mentioned procedures are, in practice, carried out by use of an electronic computer.

3. RST Wave

RST is an abbreviation of "resultant". That is to say, RST wave stands for resultant wave which is described by expressions (13) to (15). The amplitude and phase variations around the estuary are depicted respectively in Figs. 2a to 9a and Figs. 2b to 9b.*) The former is computed by $|\zeta_j|$ $(j=1, 2, 3)$ normalized by ζ_0 (the amplitude of the incident wave), the latter being calculated by $\arg \zeta_j$ $(j=1, 2, 3)$. The computed range of kd is 1.6 to 3.0. Inspection of these figures reveals the following facts. The region of high amplitude exceeding 2.0 appears along the coast facing the open sea and off-shore (refer to Fig. 10). The phenomenon is very similar to that exposed in the case of

*) Figs. 2a (2b)-7a (7b) are depicted under the 13th approximation and Fig. 8a (8b)-9a (9b) under the 15th approximation.

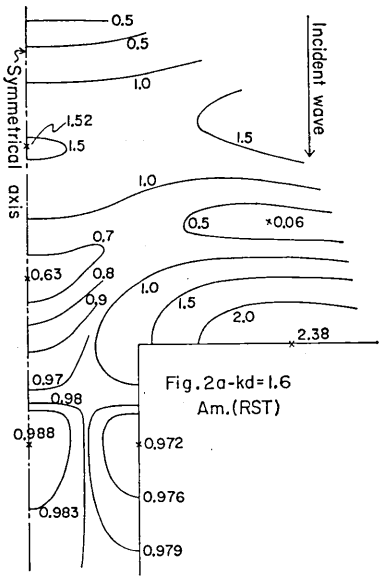

Fig. 2a. Variation of the amplitude of RST wave for kd=1.6.

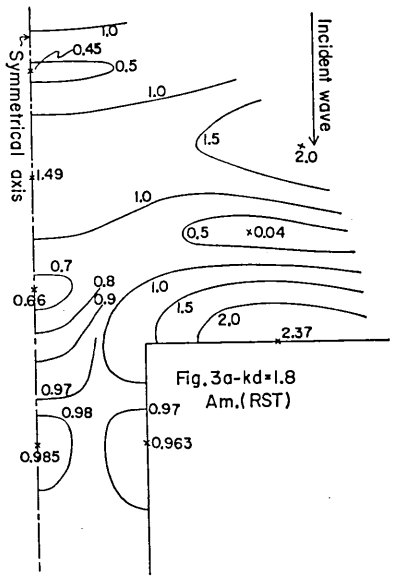

Fig. 3a. Variation of the amplitude of RST wave for kd=1.8.

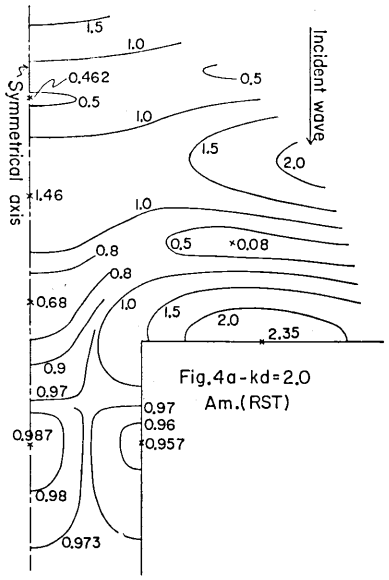

Fig. 4a. Variation of the amplitude of RST wave for kd=2.0.

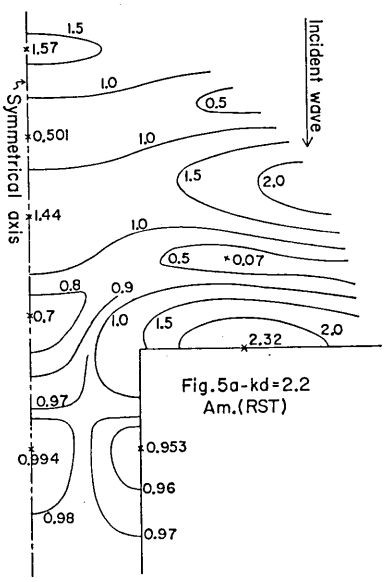

Fig. 5a. Variation of the amplitude of RST wave for kd=2.2.

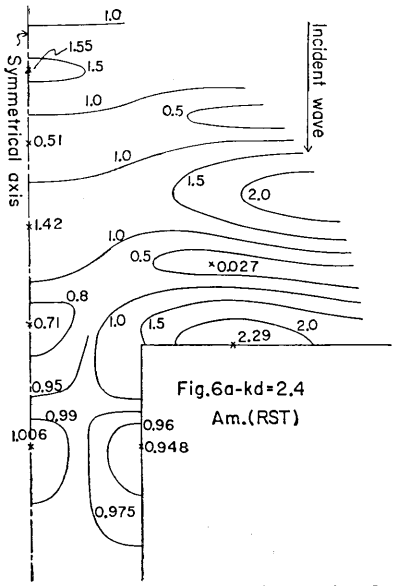

Fig. 6a. Variation of the amplitude of RST wave for kd=2.4.

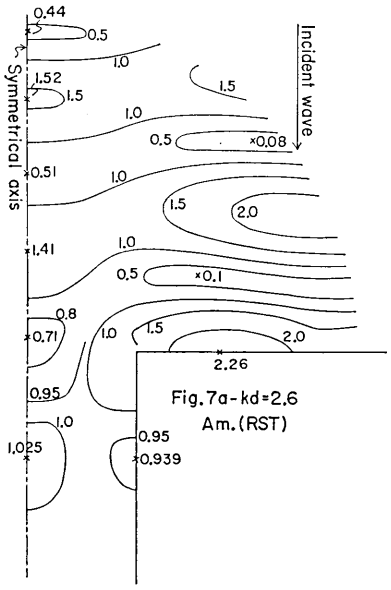

Fig. 7a. Variation of the amplitude of RST wave for kd=2.6.

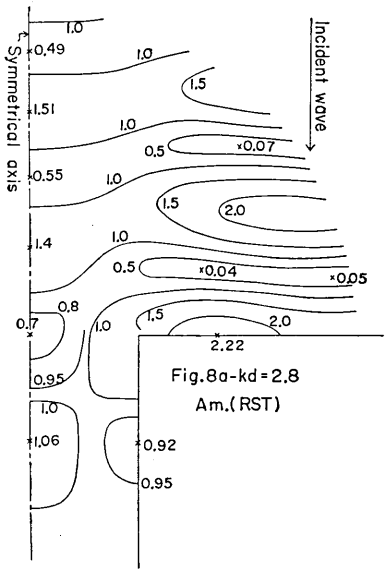

Fig. 8a. Variation of the amplitude of RST wave for kd=2.8.

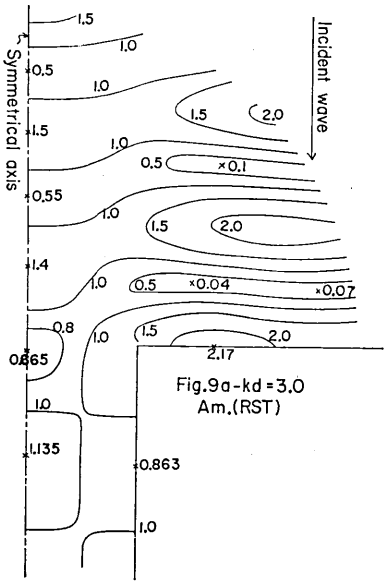

Fig. 9a. Variation of the amplitude of RST wave for kd=3.0.

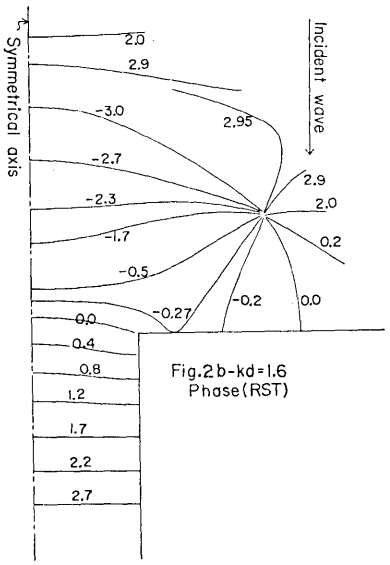

Fig. 2b. Variation of the phase of RST wave for $kd=1.6$.

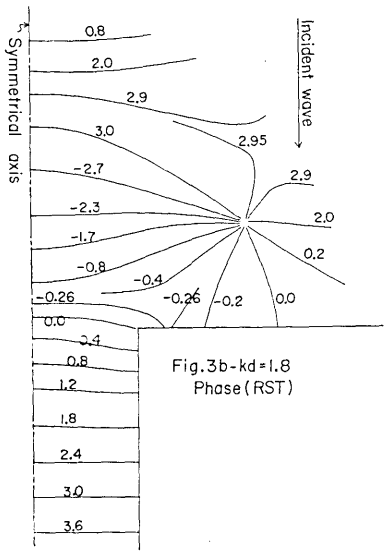

Fig. 3b. Variation of the phase of RST wave for $kd=1.8$.

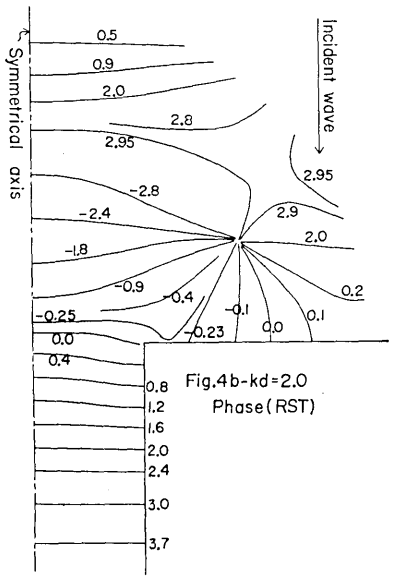

Fig. 4b. Variation of the phase of RST wave for $kd=2.0$.

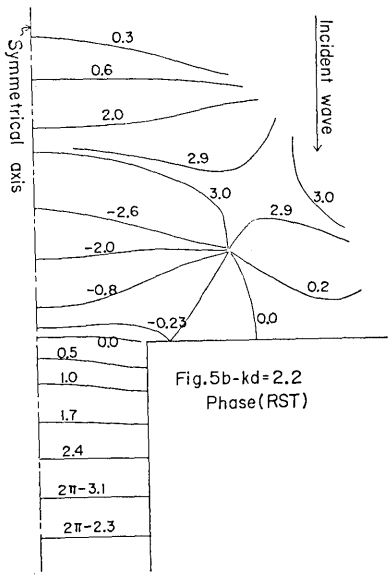

Fig. 5b. Variation of the phase of RST wave for $kd=2.2$.

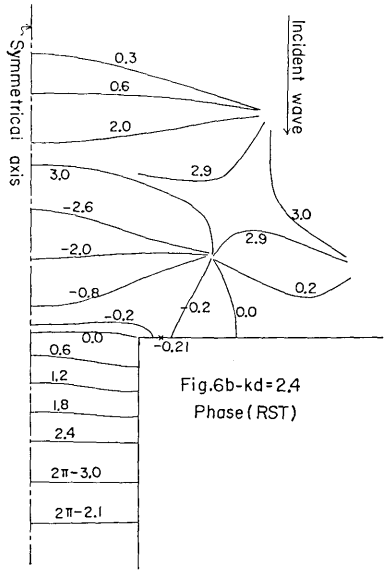

Fig. 6b. Variation of the phase of RST wave for $kd=2.4$.

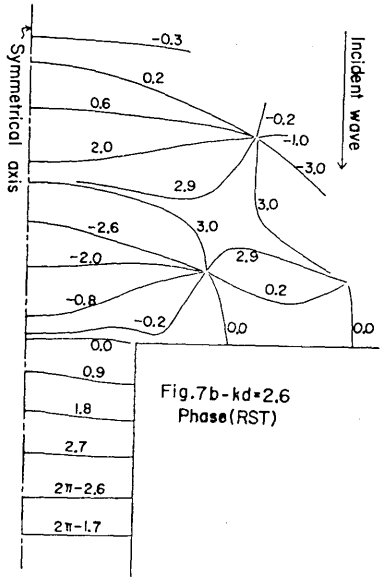

Fig. 7b. Variation of the phase of RST wave for $kd=2.6$.

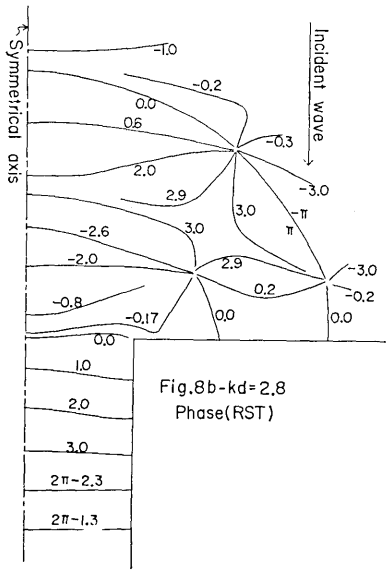

Fig. 8b. Variation of the phase of RST wave for $kd=2.8$.

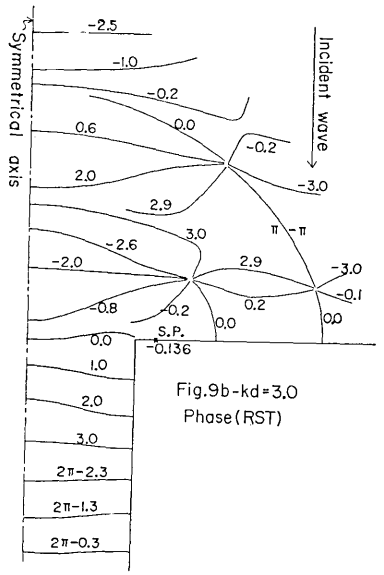

Fig. 9b. Variation of the phase of RST wave for $kd=3.0$.

the breakwater (the case of normal incidence of wave) (*Momoi*, 1967). For the generation mechanism of high wave, the same interpretation as that in the case of the breakwater might be permissible. According to the figures concerning the phase variation (Figs. 2b to 9b), the diverted and reflected wave appears in the waters near the estuary which produces the rotating wave between the invading and reflecting waves (see Fig. 11). The high wave along the coast is a result of the collision of the above-mentioned diverted wave with the coast, while the one off-shore is caused by the superposition of the diverted and reflected wave upon the wave directly reflected (refer to Fig. 12).

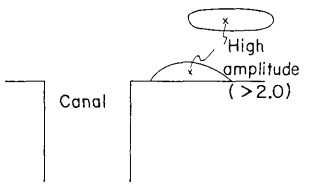

Fig. 10. Appearance of high amplitude over 2.0.

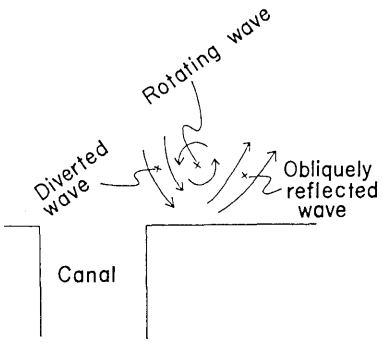

Fig. 11. Generation of rotating wave.

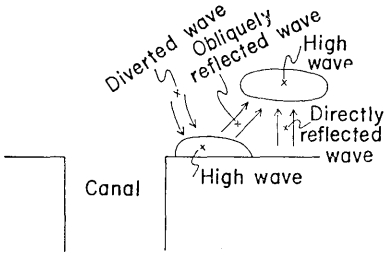

Fig. 12. Generation mechanism of high waves.

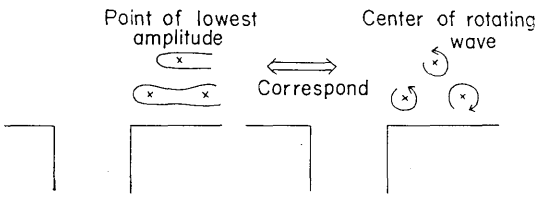

Fig. 13. Correspondence of the point of the lowest amplitude and the center of rotating wave.

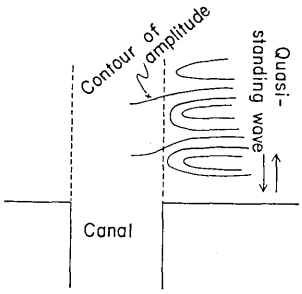

Fig. 14. Appearance of quasi-standing wave.

Comparison of the figures concerning the amplitude and phase variations shows that the point of the lowest amplitude corresponds to the center of the rotating wave (refer to Fig. 13), the feature of which is also found in the case of the breakwater (*Momoi*, 1967).

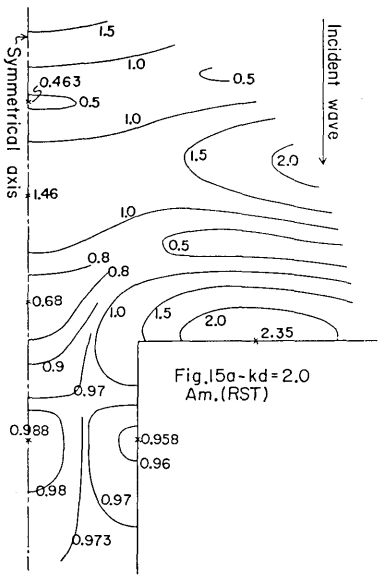

Fig. 15a. Variation of the amplitude of RST wave for $kd=2.0$ (check of convergence of the approximation used). Compare the above figure with Fig. 4a.

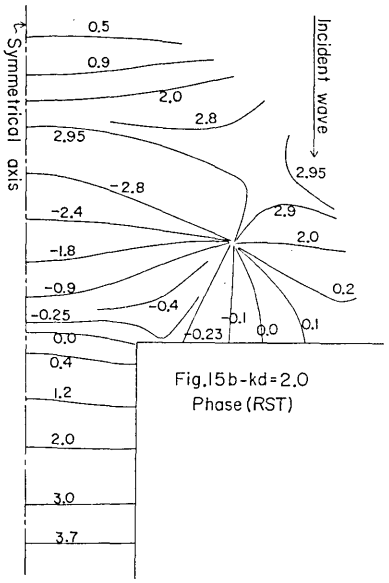

Fig. 15b. Variation of the phase of RST wave for $kd=2.0$ (check of convergence of the approximation used). Compare the above figure with Fig. 4b.

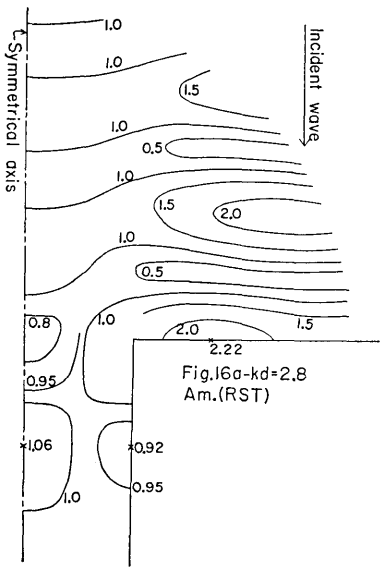

Fig. 16a. Variation of the amplitude of RST wave for $kd=2.8$ (check of convergence of the approximation used). Compare the above figure with Fig. 8a.

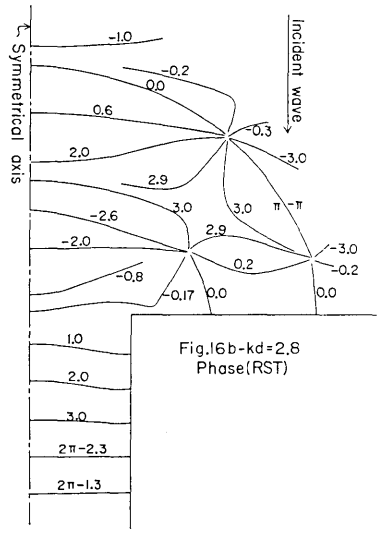

Fig. 16b. Variation of the phase of RST wave for $kd=2.8$ (check of convergence of the approximation used). Compare the above figure with Fig. 8b.

As kd increases, the feature of standing wave begins to be clearer in the waters facing the straight coast (refer to the figures of the amplitude variation). It is illustrated in Fig. 14.

According to Figs. 2b to 9b, the rotating wave in the open sea rotates with a period of the incident wave, which is also ascertained in the case of the breakwater (*Momoi*, 1967).

In Figs. 15a (15b) and 16a (16b)**), the convergence check is made. These figures denote that the convergence of the employed approximation is good enough to discuss the behavior of wave around the estuary.

4. RD Wave

As already mentioned in paper IV, the RD wave expressed by

$$\zeta_{rd}^{(j)}=\zeta_j-\zeta_0 \exp(-iky) \qquad (j=1, 2, 3)\ ,$$

where the notations used are the same as those in paper IV. The amplitude and phase variations are shown respectively in Figs. 17a to

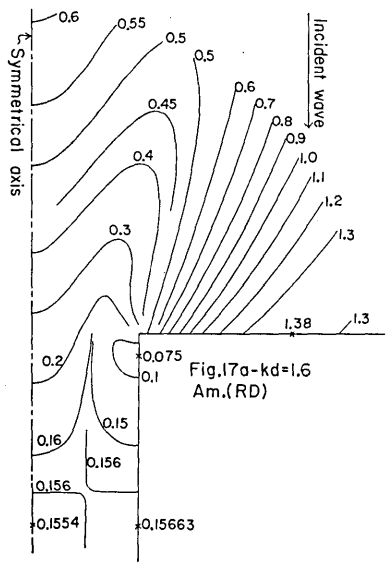

Fig. 17a. Variation of the amplitude of RD wave for $kd=1.6$.

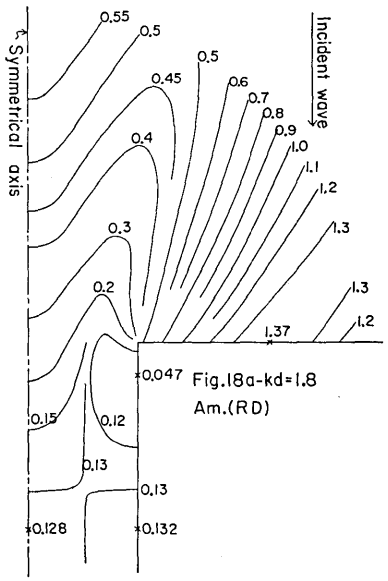

Fig. 18a. Variation of the amplitude of RD wave for $kd=1.8$.

**) Fig. 15a (15b) is based on the 15th approximation and Fig. 16a (16b) on the 13th approximation.

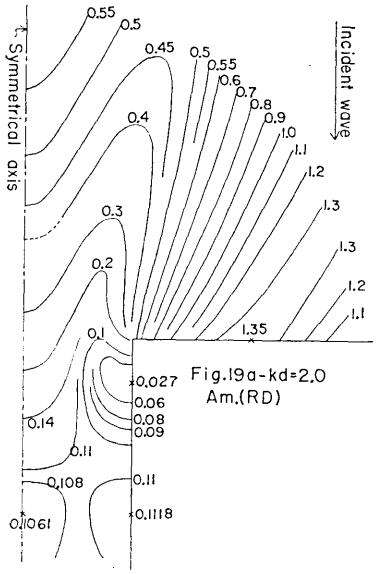

Fig. 19a. Variation of the amplitude of RD wave for $kd=2.0$.

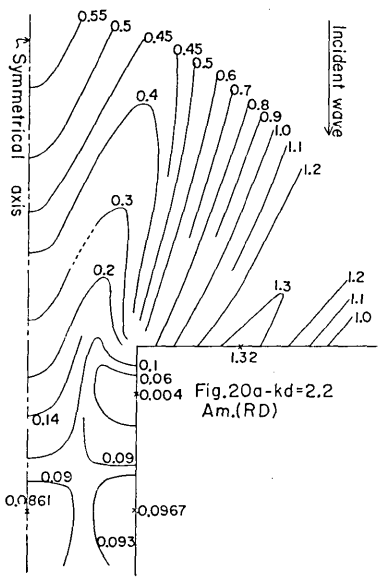

Fig. 20a. Variation of the amplitude of RD wave for $kd=2.2$.

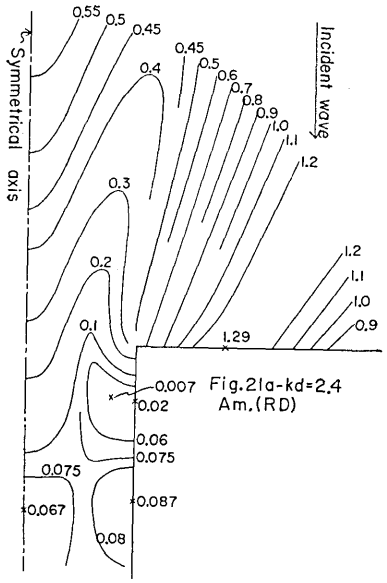

Fig. 21a. Variation of the amplitude of RD wave for $kd=2.4$.

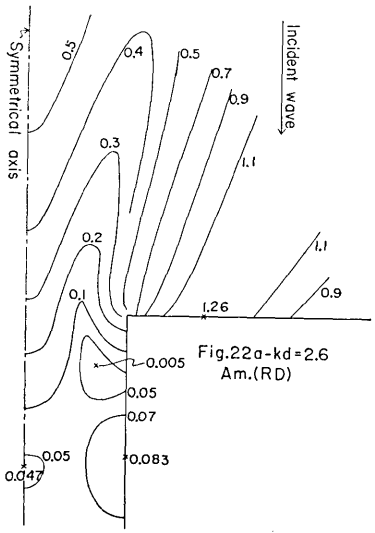

Fig. 22a. Variation of the amplitude of RD wave for $kd=2.6$.

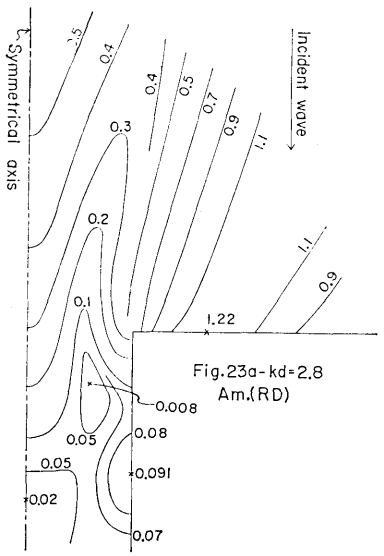

Fig. 23a. Variation of the amplitude of RD wave for $kd=2.8$.

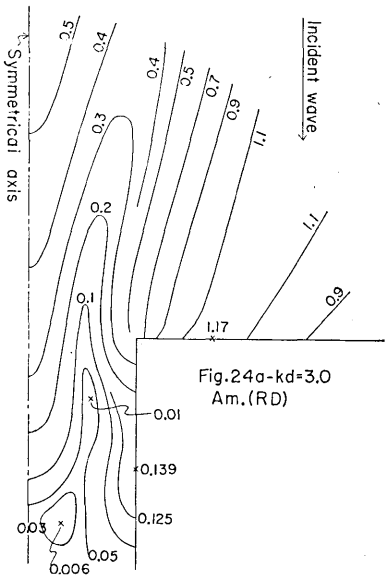

Fig. 24a. Variation of the amplitude of RD wave for $kd=3.0$.

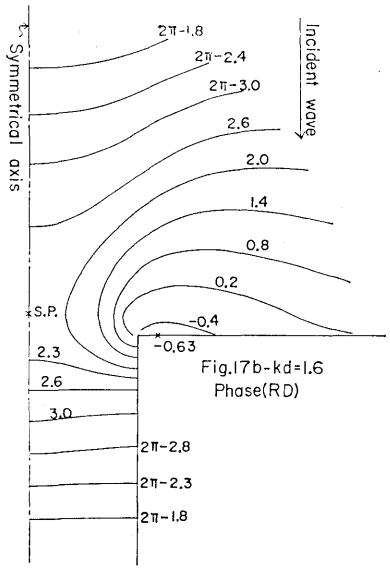

Fig. 17b. Variation of the phase of RD wave for $kd=1.6$.

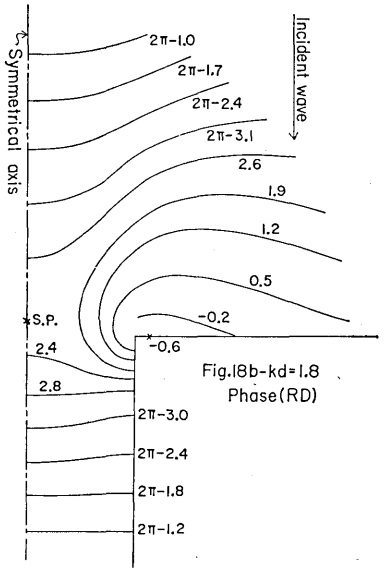

Fig. 18b. Variation of the phase of RD wave for $kd=1.8$.

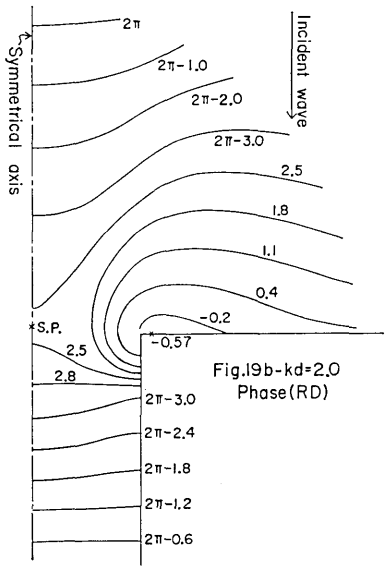

Fig. 19b. Variation of the phase of RD wave for $kd=2.0$.

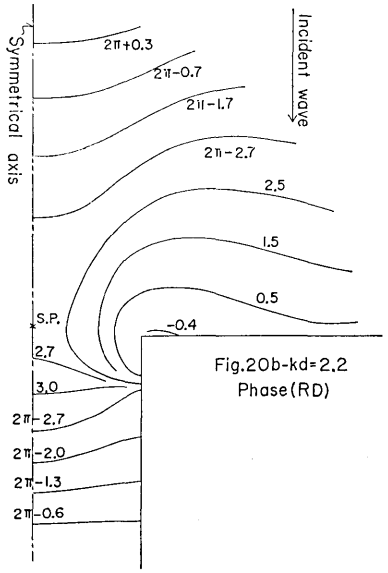

Fig. 20b. Variation of the phase of RD wave for $kd=2.2$.

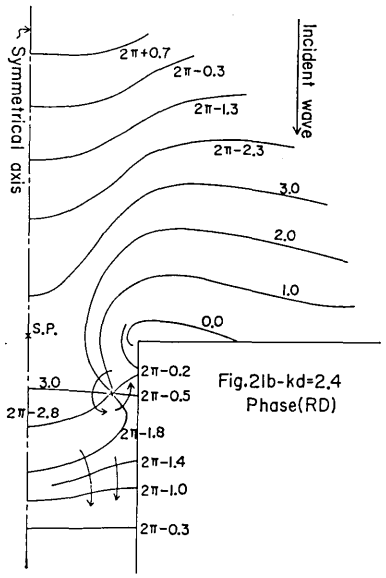

Fig. 21b. Variation of the phase of RD wave for $kd=2.4$.

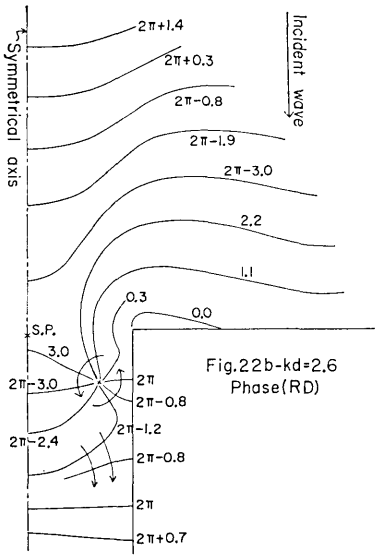

Fig. 22b. Variation of the phase of RD wave for $kd=2.6$.

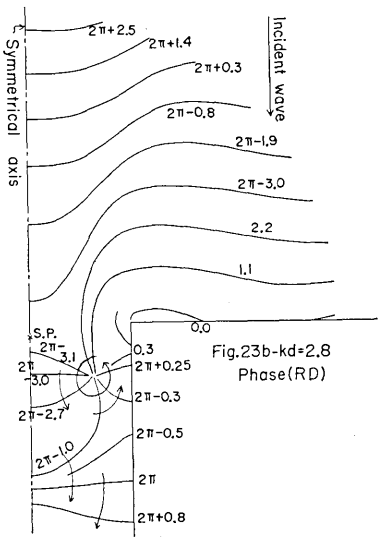

Fig. 23b. Variation of the phase of RD wave for $kd=2.8$.

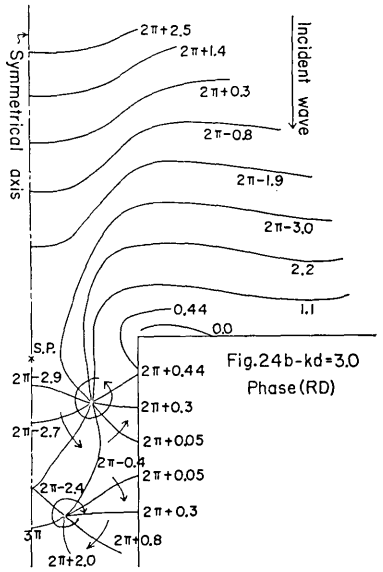

Fig. 24b. Variation of the phase of RD wave for $kd=3.0$.

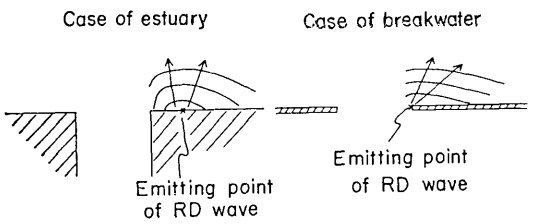

Fig. 25. Difference of the emitting points of RD wave in the cases of the estuary and breakwater.

24a and Figs. 17b to 24b.***) The computed range of kd is 1.6 to 3.0. The numerals stated in the figures relevant to amplitude denote $|\zeta_{rd}^{(j)}|$ $(j=1, 2, 3)$ normalized by ζ_0, those concerning phase variation being arg $\zeta_{rd}^{(j)}$. According to these figures, the following facts are found.

The amplitude and phase variations of RD wave in the open sea for the case of the estuary and those in the windward waters for the case of the breakwater (normal incidence) (*Momoi*, 1967) are so alike that the discussion in the present case seems to go along the same lines as that in the case of the breakwater except for the emitting point of RD wave. The emitting point of RD wave in the case of the former is a point slightly away from the corner of the estuary, while that in the latter is, according to the result of numerical experiment,

***) Figs. 17a (17b)-22a (22b) are depicted under the 13th approximation and Figs. 23a (23b)-24a (24b) under the 15th approximation.

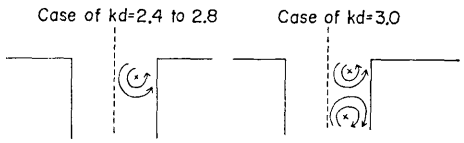

Fig. 26. Appearance of rotating wave in the canal.

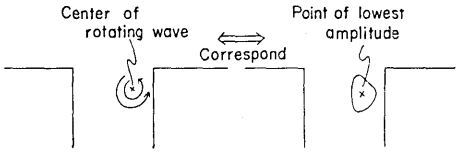

Fig. 27. Correspondence of the center of rotating wave and the point of the lowest amplitude.

a terminus of the breakwater wing (refer to Fig. 25).

A conspicuous feature of the phase variation in the canal is an appearance of rotating wave for kd over about 2.2 (refer to Figs. 21b to 24b and Fig. 26, i.e. the figurative explanation). The above rotating wave is a phenomenon peculiar to the waters of the canal of estuary. It will be shown in the later section concerning the variation of RD wave around a right-angled corner. Comparing Figs. 21a to 24a with Figs. 21b to 24b, the center of the rotating wave corresponds to the point of the lowest amplitude (refer to Fig. 27).

5. Decaying Mode

In this section, the numerical calculation for the decaying mode in the canal is carried out. Since the calculated range is, for the present, $kd<\pi$, the decaying mode is expressed as

$$\zeta_{decay}=\sum_{m=1}^{\infty}\zeta_1^{(m)}\cos\frac{m\pi}{d}x\cdot e^{-ik_1^{(m)}y}\,, \tag{16}$$

where

$$\zeta_1=\zeta_{adv}+\zeta_{decay}\,,\qquad \zeta_{adv}=\zeta_1^{(0)}e^{-iky}\,.$$

The above expression (16) denotes the *reflecting* behavior of the waves which invade the canal. The calculated results of the amplitude are arranged in Figs. 28a for $kd=0.02$ to 2.2 and in Fig. 29a for $kd=2.4$ to 3.0, those of the phase being shown in Figs. 28b for $kd=0.02$ to 2.2 and in Fig. 29b for $kd=2.4$ to 3.0. The calculations of the amplitude and phase are based on $|\zeta_{decay}/\zeta_0|$ and $\arg\zeta_{decay}$.

In Figs. 28a and 29a, the growing nature of standing wave (first mode) is found in the canal with increase of the value of kd from 0 to π.

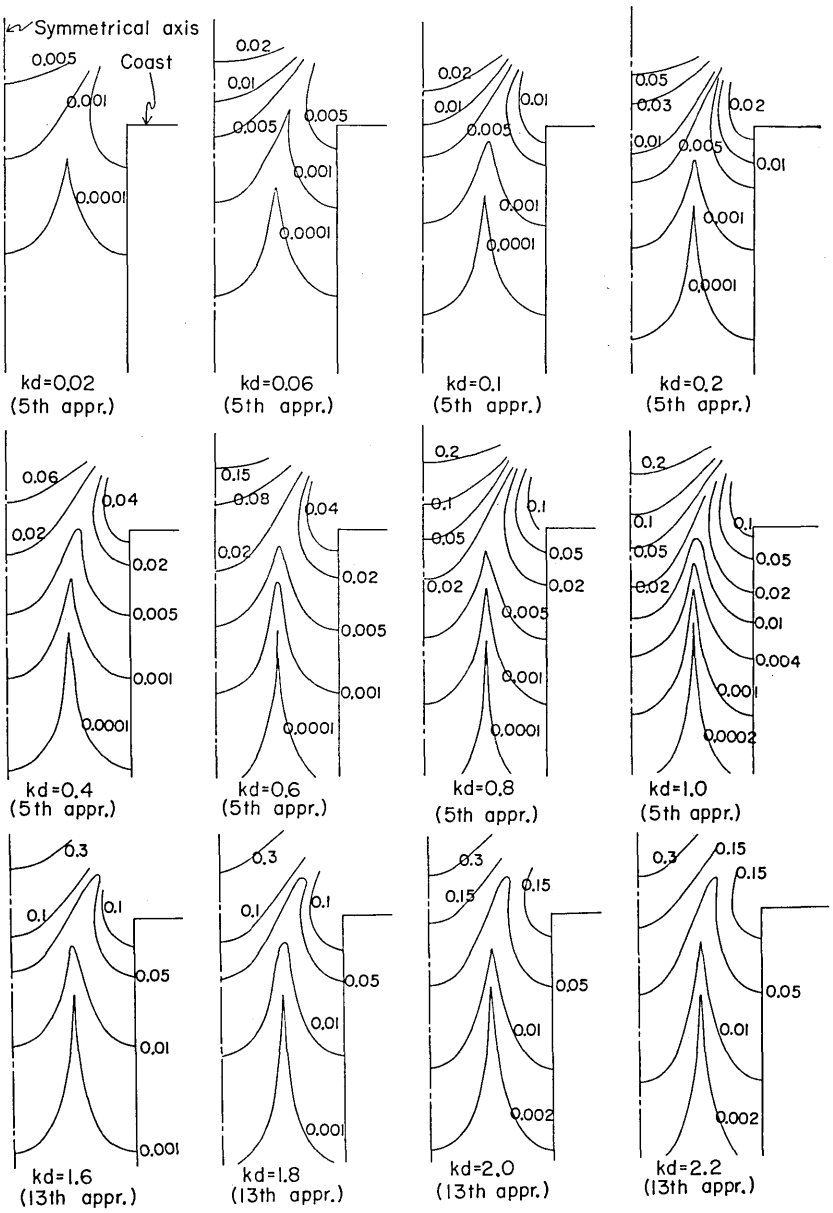

Fig. 28a. Variation of the amplitude of the decaying modes in the canal for $kd=0.02$ to 2.2.

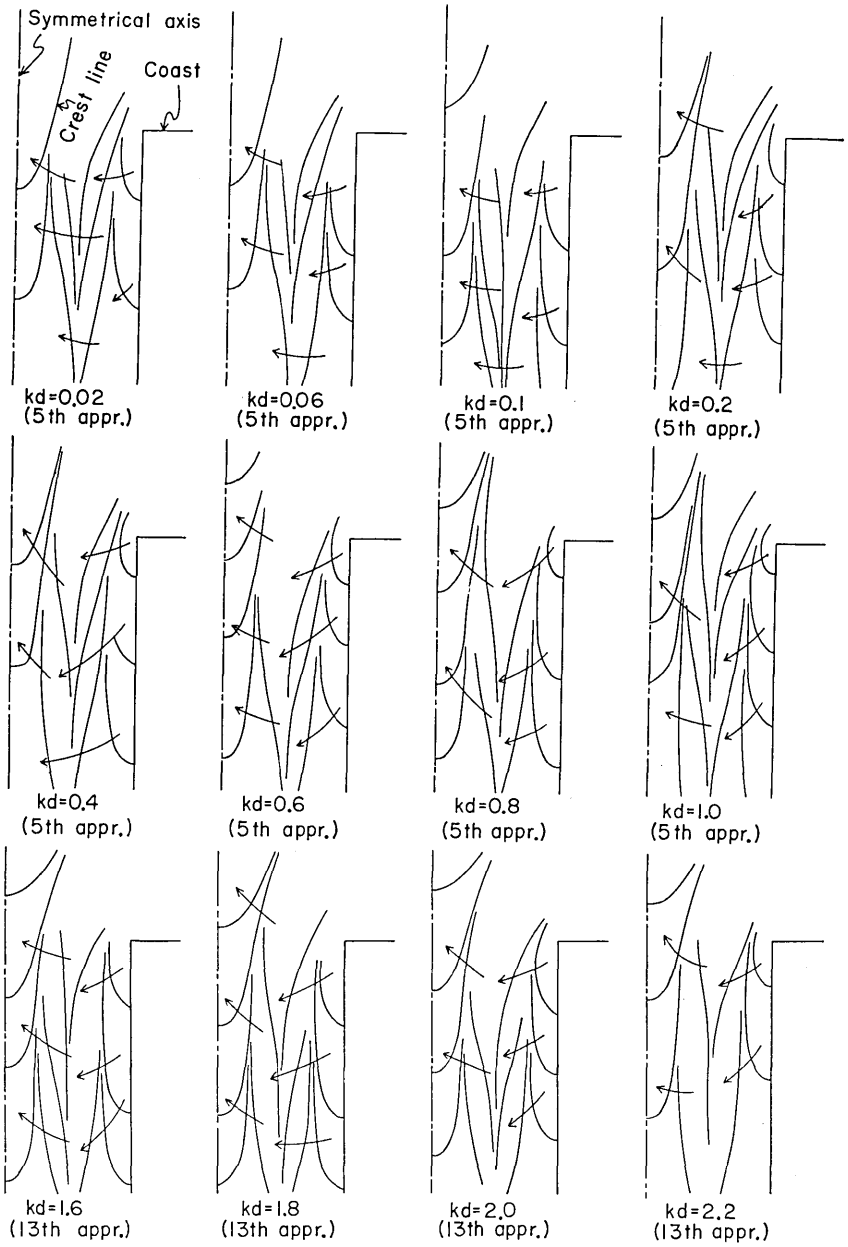

Fig. 28b. Variation of the phase of the decaying modes in the canal for $kd=0.02$ to 2.2.

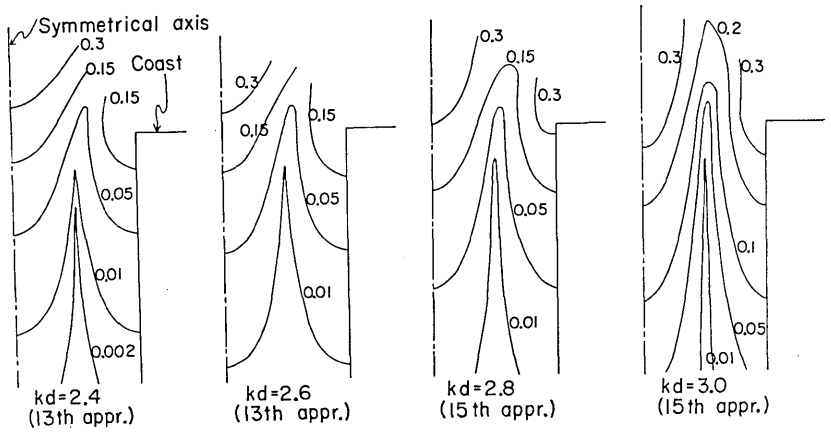

Fig. 29a. Variation of the amplitude of the decaying modes in the canal for $kd=2.4$ to 3.0.

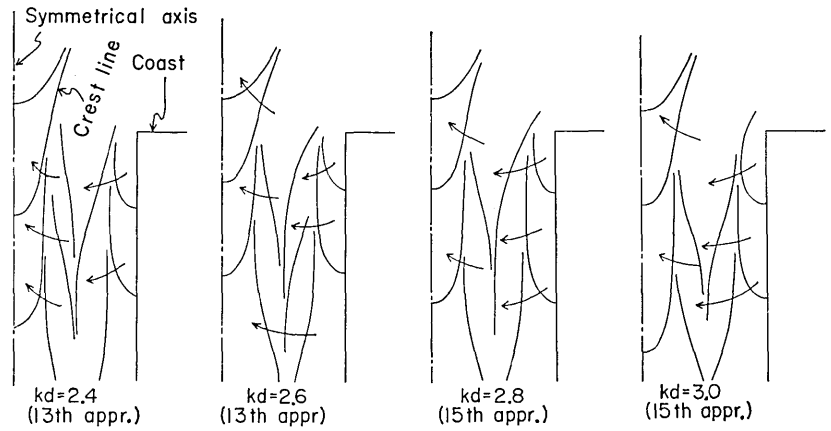

Fig. 29b. Variation of the phase of the decaying modes in the canal for $kd=2.4$ to 3.0.

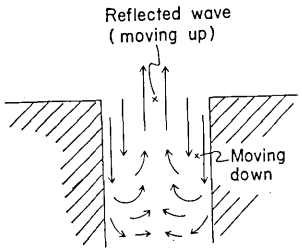

Fig. 30. Behavior of the reflecting wave in the canal.

According to Figs. 28b and 29b, the reflecting wave (from the canal to the open sea) moves up in the middle part of the canal, the waves moving down along the banks of the canal as the counter flow of the above reflecting wave (refer to Fig. 30).

6. Waves around the Right- angled Corner

When a train of periodic wave

$$\zeta_{in}=\zeta_0 \exp(i\omega t+iky)$$

(ζ_0: the amplitude of the incident wave, ω: the angular frequency, t: the time variable, k: the wave number, and y: the y-component of the cartesian coordinate) invades the right-angled corner (for the geometry of the model used, Fig. 31 should be referred to), the solution of the wave equation

$$\frac{\partial^2\zeta}{\partial x^2}+\frac{\partial^2\zeta}{\partial y^2}=\frac{1}{c^2}\frac{\partial^2\zeta}{\partial t^2}$$

(x: the x-component of the cartesian coordinate, ζ: the wave height, and c: the velocity of the long wave) is readily obtained, after the procedure developed by Stoker (*Stoker*, 1965) for the model of a single breakwater wing, as follows.

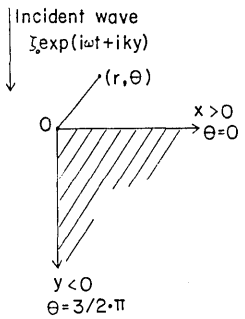

Fig. 31. Model of the right-angled corner.

$$\zeta/\zeta_0=\frac{4}{3}J_0(kr)+\frac{8}{3}\sum_{n=1}^{\infty}\exp\left(i\frac{n\pi}{3}\right)\cos\frac{n\pi}{3}\cos\frac{2}{3}n\theta J_{2n/3}(kr)\,, \qquad (17)$$

where r and θ are the polar coordinate, the time factor being omitted as usual (the derivation of the above solution is detailed in Mitsui's work (*Mitsui*, 1967)).

Using expression (17), the amplitude and phase variations are depicted, respectively, in Figs. 32a to 36a and in Figs. 32b to 36b for the range of $kr=0.002$ to 15.0.[†] Inspection of these figures reveals that: (i) the wave exceeding 2.0 in amplitude appears along the coast exposed to the incident wave and in the offing (refer to the shaded regions in Figs. 35a and 36a), and (ii) rows of rotating waves appear also in the windward waters facing the windward coast (refer to Figs. 35b and 36b).

The variations of the amplitude and phase of RD wave

$$\zeta_{rd}=\zeta-\zeta_0 \exp(iky) \qquad (18)$$

[†] The amplitude and phase variations are depicted by use of $|\zeta/\zeta_0|$ and $\arg\zeta/\zeta_0$.

(the time factor is omitted as usual), which denotes the purely reflected and diffracted wave excluding the incident wave from (17), are shown

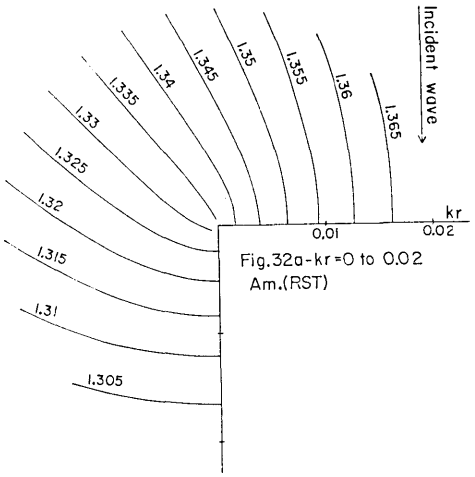

Fig. 32a. Variation of the amplitude of RST wave around the right-angled corner for $kr=0$ to 0.02.

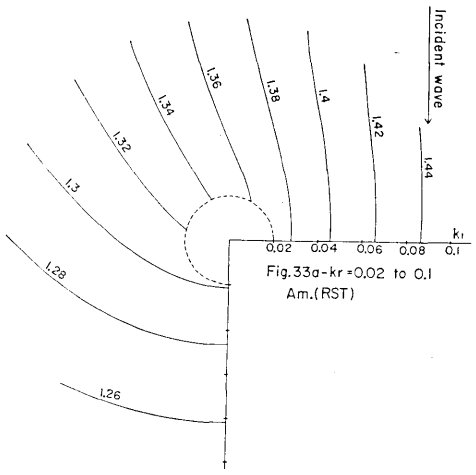

Fig. 33a. Variation of the amplitude of RST wave around the right-angled corner for $kr=0.02$ to 0.1.

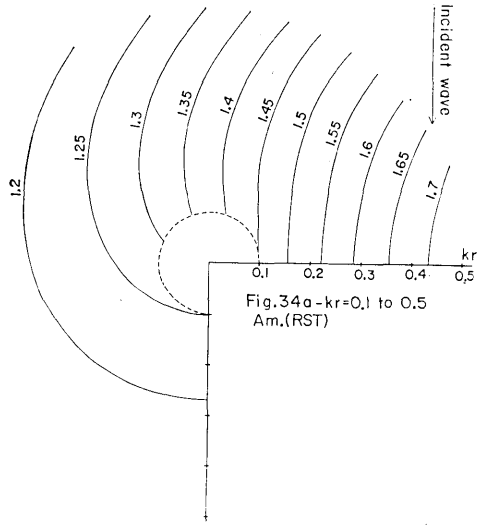

Fig. 34a. Variation of the amplitude of RST wave around the right-angled corner for $kr=0.1$ to 0.5.

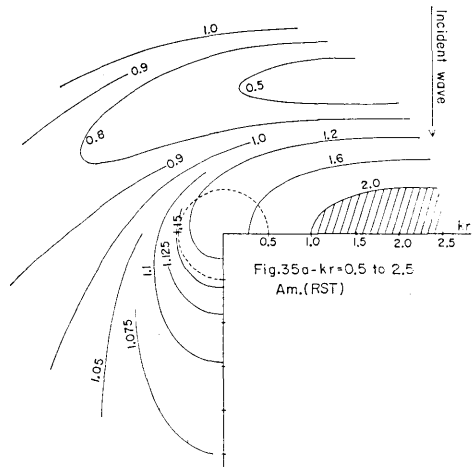

Fig. 35a. Variation of the amplitude of RST wave around the right-angled corner for $kr=0.5$ to 2.5.

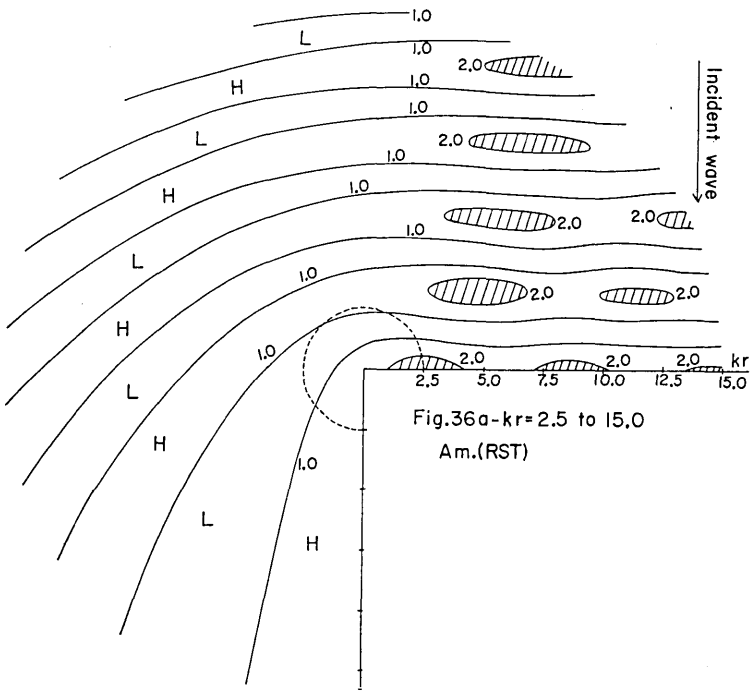

Fig. 36a. Variation of the amplitude of RST wave around the right-angled corner for kr=2.5 to 15.0.

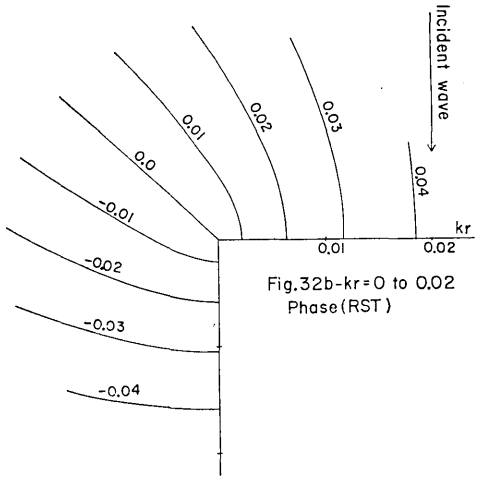

Fig. 32b. Variation of the phase of RST wave around the right-angled corner for kr=0 to 0.02.

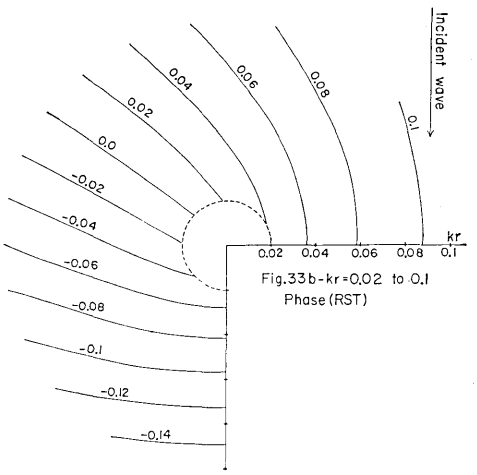

Fig. 33b. Variation of the phase of RST wave around the right-angled corner for kr=0.02 to 0.1.

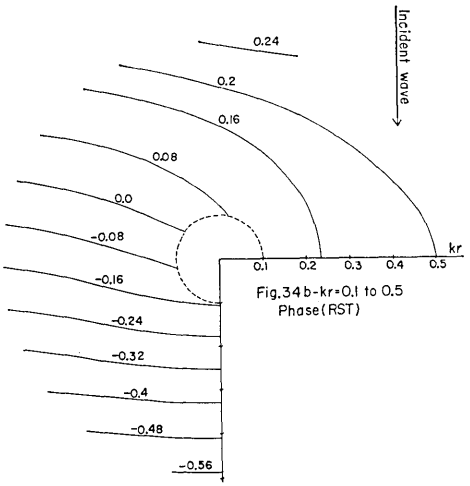

Fig. 34b. Variation of the phase of RST wave around the right-angled corner for kr=0.1 to 0.5.

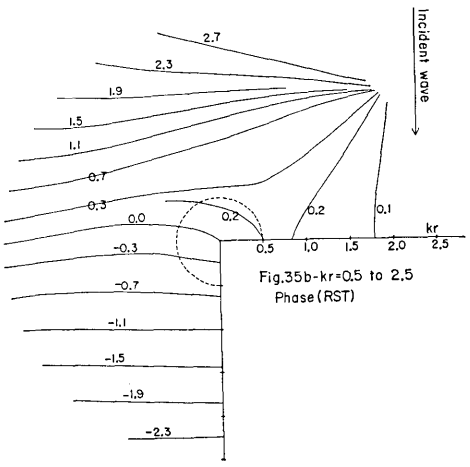

Fig. 35b. Variation of the phase of RST wave around the right-angled corner for kr=0.5 to 2.5.

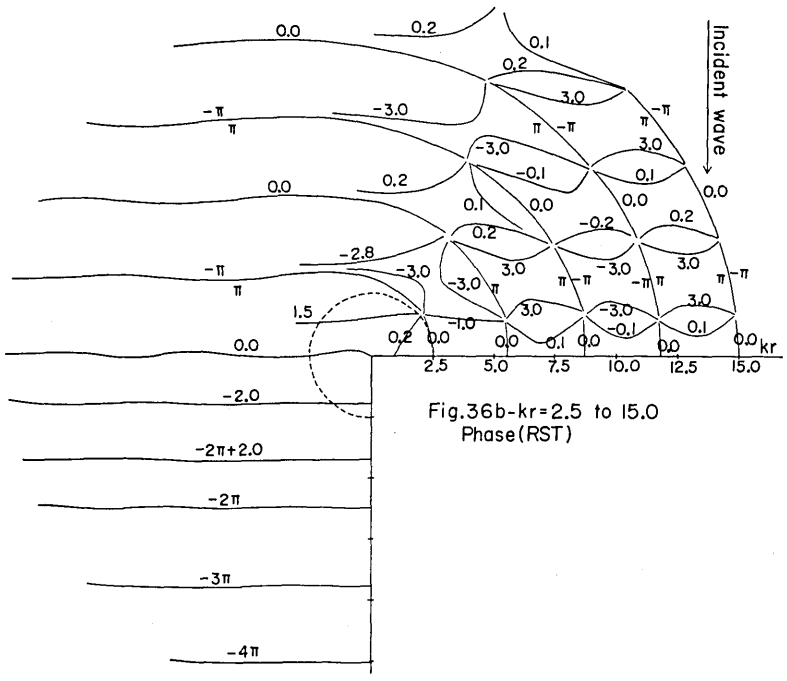

Fig. 36b. Variation of the phase of RST wave around the right-angled corner for kr=2.5 to 15.0.

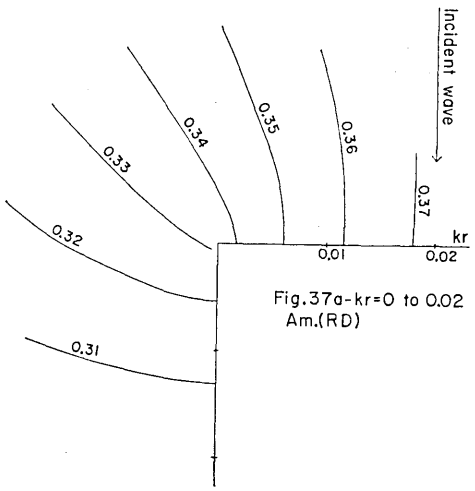

Fig. 37a. Variation of the amplitude of RD wave around the right-angled corner for kr=0 to 0.02.

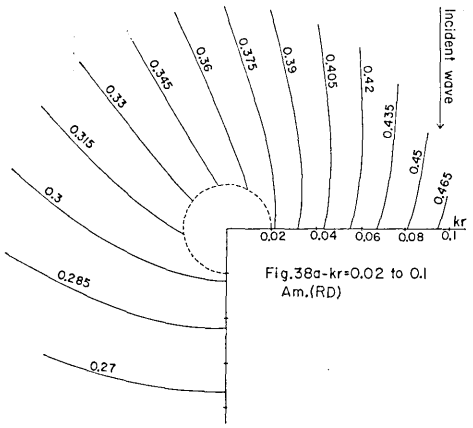

Fig. 38a. Variation of the amplitude of RD wave around the right-angled corner for kr=0.02 to 0.1.

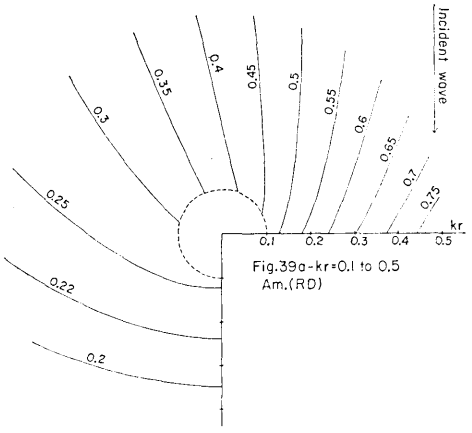

Fig. 39a. Variation of the amplitude of RD wave around the right-angled corner for kr=0.1 to 0.5.

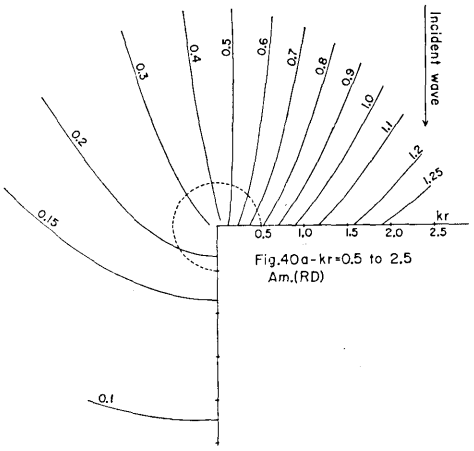

Fig. 40a. Variation of the amplitude of RD wave around the right-angled corner for kr=0.5 to 2.5.

in Figs. 37a to 41a and 37b to 41b.[††] The variations of the amplitude and phase in the present case are very similar to those in the case of the estuary (refer to Section 4). That is to say, (iii) a packet of wave

[††] The numerals stated in the figures denote $|\zeta_{rd}/\zeta_0|$ in Figs. 37a to 41a and $\arg \zeta_{rd}/\zeta_0$ in Figs. 37b to 41b.

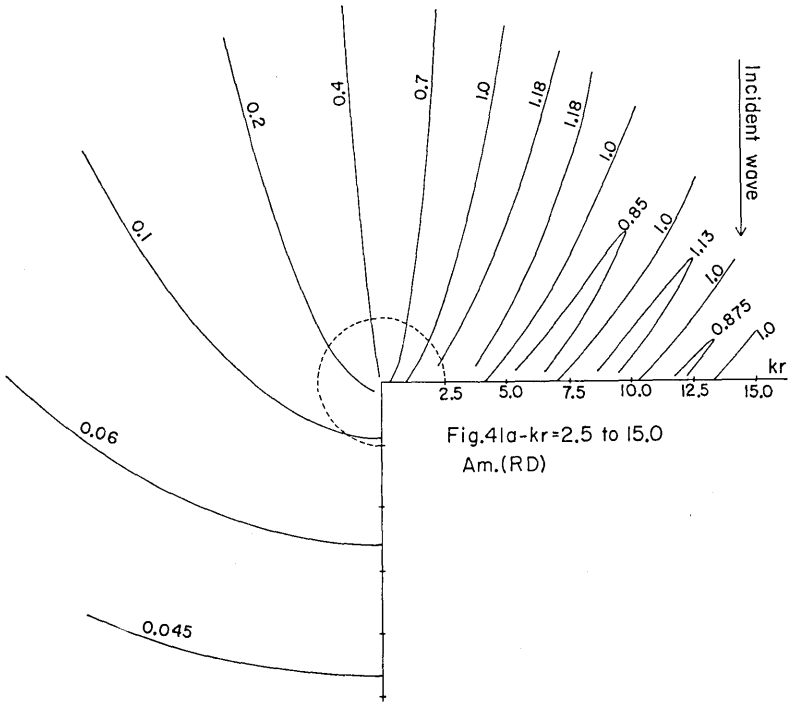

Fig. 41a. Variation of the amplitude of RD wave around the right-angled corner for kr=2.5 to 15.0.

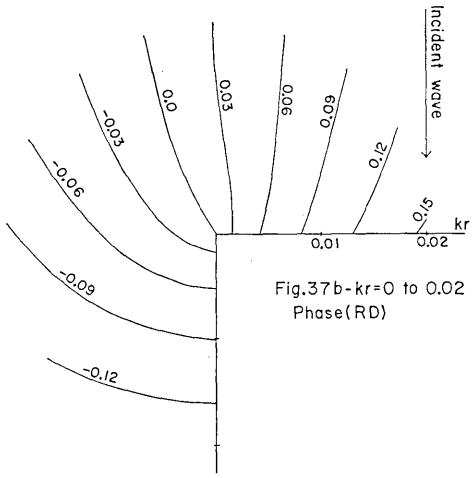

Fig. 37b. Variation of the phase of RD wave around the right-angled corner for kr=0 to 0.02.

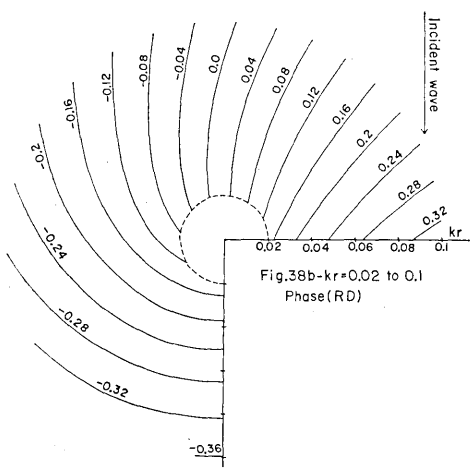

Fig. 38b. Variation of the phase of RD wave around the right-angled corner for kr=0.02 to 0.1.

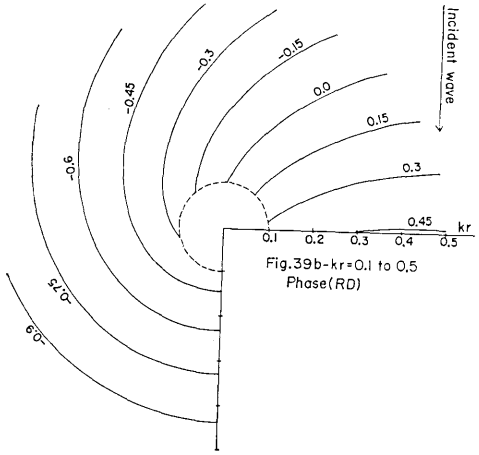

Fig. 39b. Variation of the phase of RD wave around the right-angled corner for kr=0.1 to 0.5.

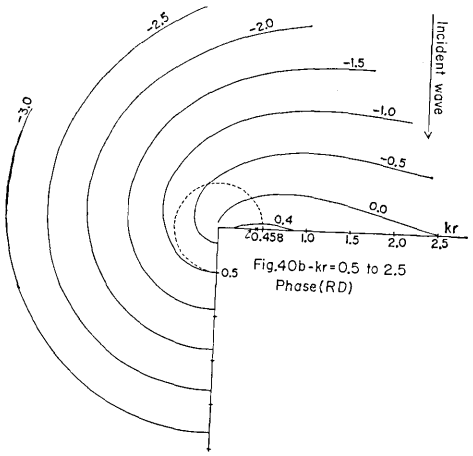

Fig. 40b. Variation of the phase of RD wave around the right-angled corner for kr=0.5 to 2.5.

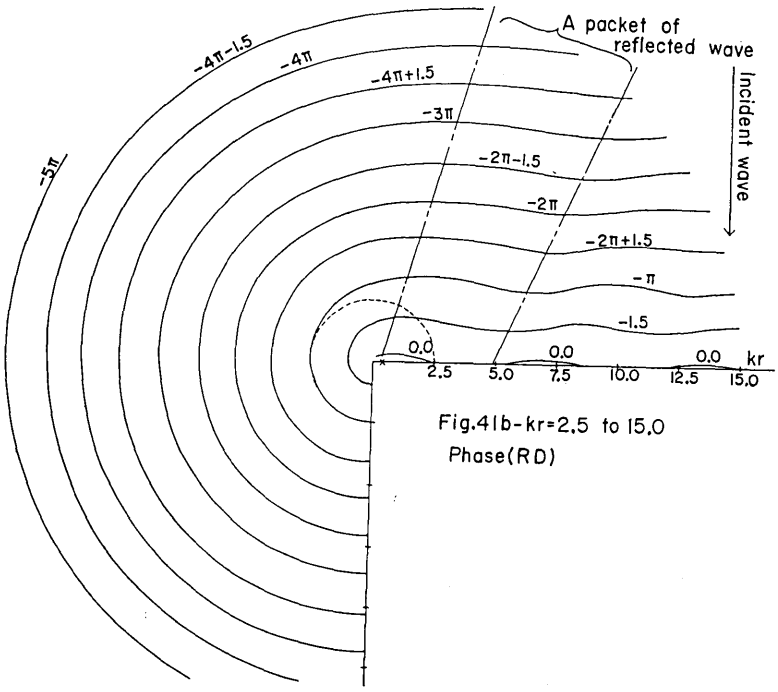

Fig. 41b. Variation of the phase of RD wave around the right-angled corner for kr=2.5 to 15.0.

is found which is reflected at the coast near the corner to move away toward the open sea. The above packet of wave accompanies a complementary flow along the neighbouring region of the packet. These phenomena are illustrated in Fig. 42. The above-mentioned three phenomena (i), (ii) and (iii) show definitely that the generation mechanisms of high waves (>2.0) and the rotating waves in the open sea for the case of the estuary be not caused as the result of the coupling of waves diffracted from two corners of the estuary.

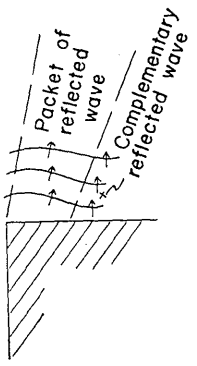

Fig. 42. Illustration of a wave packet and the complementary flow.

As shown in Figs. 37b to 41b, a rotating wave such as that appearing in the canal of the estuary for RD wave does not appear, but the wave in the leeward waters advances monotonically. From this fact, the rotating wave in the canal of the estuary is interpreted to be the result of the multi-reflection of the diffracted waves (from two corners of the estuary) in the canal.

7. Solution by the Method of Mirror Image

The coupling effect of two coasts of the estuary, one of which extends along the positive x-axis and the other along the negative one (refer to Fig. 1), begins to be small as the wave-length of the incident wave becomes small for the width of the canal. Construction of mirror image of the single right-angled corner (the model used in the foregoing Section 6) with respect to the line parallel to the leeward edge, therefore, makes possible the investigation of the wave around the estuary with comparatively medium to small wave-length compared with the width of the canal. Referring to Fig. 43, the origin is located at the corner of the right-hand model, the coordinate of the corner of the image being $(-2d, 0)$ in the cartesian coordinate. Let $\zeta_0 \exp(i\omega t + iky)$ be the incident wave (the same notations as those in Section 6 are used). The

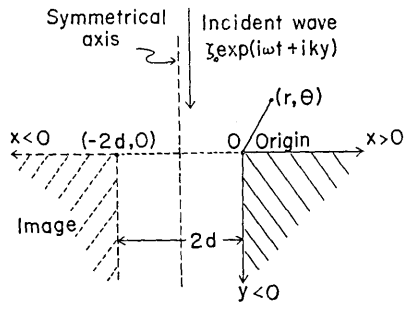

Fig. 43. Geometry of the model used on the basis of the method of mirror image.

reflected and diffracted (RD) wave from the right-hand corner is given by (18) in Section 6, i.e.,

$$\zeta_{rd}^{right}=\zeta^{right}-\zeta_0 \exp(iky) , \tag{19}$$

where super-suffix *'right'* denotes the quantities relevant to the right-hand corner, ζ^{right} being expressed in (17). Since the corner point of the left-hand (image) model is located at the coordinate $(-2d, 0)$ with the windward coast extending along the x-axis to the negative direction, the resultant (RST) wave for the image model is given by

$$\zeta^{left}=\frac{4}{3}J_0(kr')+\frac{8}{3}\sum_{n=1}^{\infty}\exp\left(i\frac{n\pi}{3}\right)\cos\frac{n\pi}{3}\cos\frac{2}{3}n\theta' J_{2n/3}(kr') , \tag{20}$$

where

$$r'=\sqrt{r^2+4rd\cos\theta+4d^2} ,$$

$$\theta'=\tan^{-1}(y'/x') ,$$

$$x'=-r\cos\theta-2d ,$$

$$y'=y=r\sin\theta .$$

The wave reflected and diffracted from the image model (ζ_{rd}^{left}) is then (using (20))

$$\zeta_{rd}^{left}=\zeta^{left}-\zeta_0 \exp(iky) . \tag{21}$$

The solution by the method of mirror image is now described, by using (19) and (21), as follows.

$$\zeta_{rst}^{mirror}=\zeta_{rd}^{right}+\zeta_{rd}^{left}+\zeta_0 \exp(iky) , \tag{22}$$

where ζ_{rst}^{mirror} stands for the wave height of the resultant wave by the method of mirror image, the last term $\zeta_0 \exp(iky)$ being the incident wave.

The solution of the reflected and diffracted wave by this method (ζ_{rd}^{mirror}) is then

$$\zeta_{rd}^{mirror}=\zeta_{rd}^{right}+\zeta_{rd}^{left} , \tag{23}$$

which is the form excluding the incident wave from the resultant wave (22).

In the solution by the present method, only the primary reflection is taken into account, the higher order reflections (secondary and tertiary

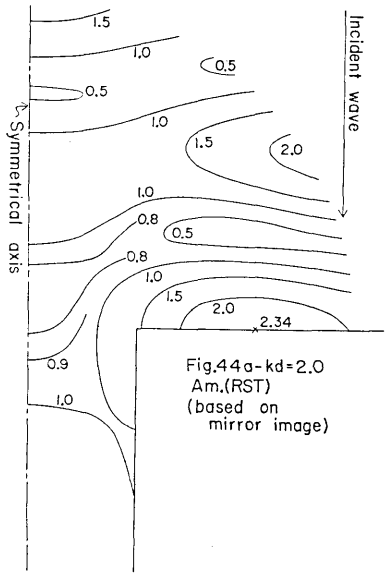

Fig. 44a. Variation of the amplitude of RST wave around the estuary for $kd=2.0$ (based on the method of mirror image).

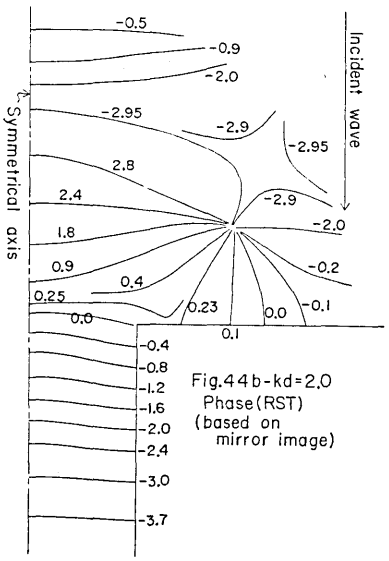

Fig. 44b. Variation of the phase of RST wave around the estuary for $kd=2.0$ (based on the method of mirror image).

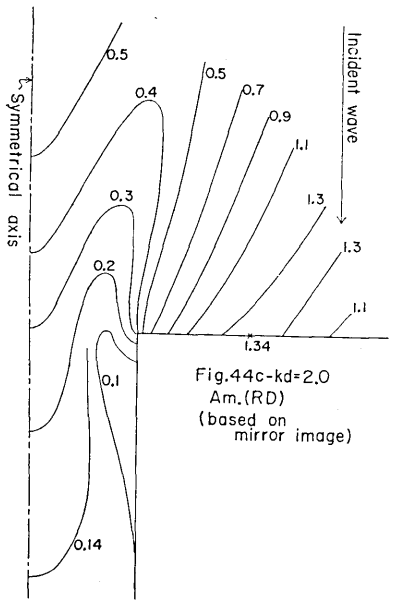

Fig. 44c. Variation of the amplitude of RD wave around the estuary for $kd=2.0$ (based on the method of mirror image).

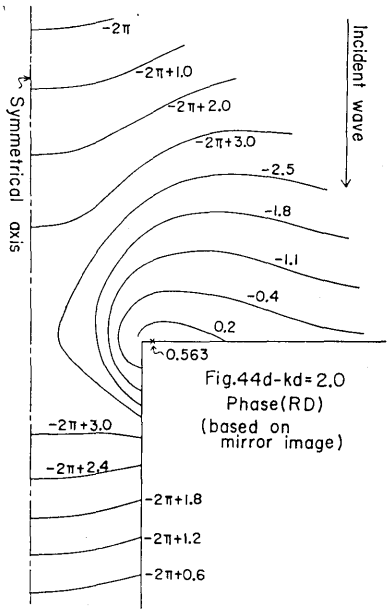

Fig. 44d. Variation of the phase of RD wave around the estuary for $kd=2.0$ (based on the method of the mirror image).

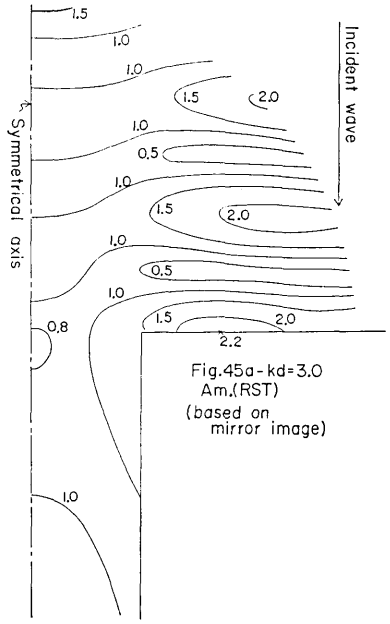

Fig. 45a. Variation of the amplitude of RST wave around the estuary for $kd=3.0$ (based on the method of mirror image).

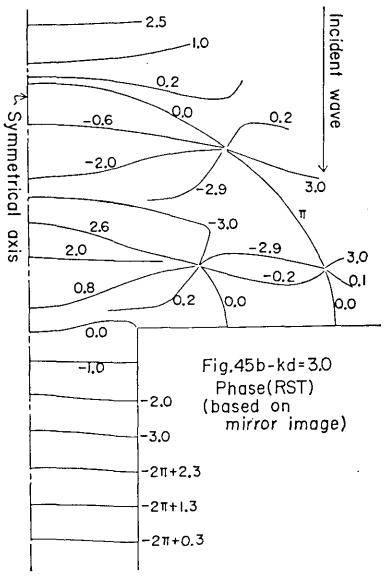

Fig. 45b. Variation of the phase of RST wave around the estuary for $kd=3.0$ (based on the method of mirror image).

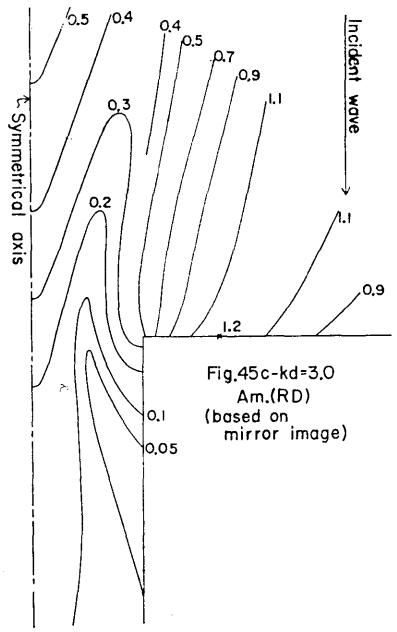

Fig. 45c. Variation of the amplitude of RD wave around the estuary for $kd=3.0$ (based on the method of mirror image).

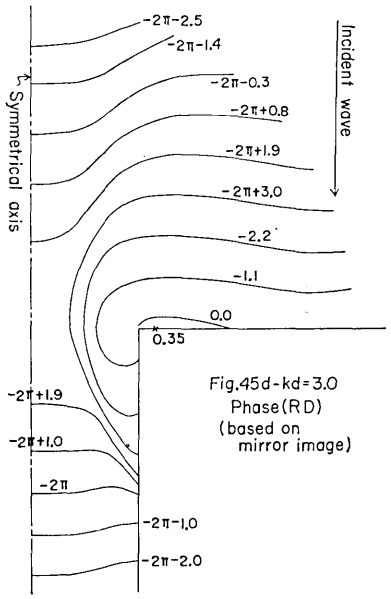

Fig. 45d. Variation of the phase of RD wave around the estuary for $kd=3.0$ (based on the method of mirror image).

ones) being neglected. The higher order reflections might be more striking in the canal than in the open sea.

Using the expressions (22) and (23), the variations of the amplitude and phase are depicted in Figs. 44a to 44d for $kd=2.0$ and Figs. 45a to 45d for $kd=3.0$. The stated values in the figures denote $|\zeta_{rst}^{mirror}/\zeta_0|$ in Figs. 44a–45a, $\arg \zeta_{rst}^{mirror}$ in Figs. 44b–45b, $|\zeta_{rd}^{mirror}/\zeta_0|$ in Figs. 44c–45c and $\arg \zeta_{rd}^{mirror}$ in Figs. 44d–45d.

Comparison of the above figures with those in Sections 3 and 4 (Figs. 4a, 4b, 9a, 9b, 19a, 19b, 24a and 24b) reveals that the agreement of the variation of these figures (the former is based on the method of mirror image and the latter on the rigorous method) is fairly good in the area of the open sea with disappearing tendency towards the inside of the canal. Since only the primary reflection is, as already mentioned, taken into account in the method of mirror image, the good agreement in the open sea indicates that the behavior of the wave for $kd \gtrsim 2.0$ in the open sea can be explained as the result of only the primary reflection of the incident wave. On the other hand, the disagreement in the part of the canal suggests the predominance of the secondary reflection. Comparing the phase variation of RD wave in the canal based on the mirror image method (Fig. 45d) and that on the rigorous method (Fig. 24b), it turns out that the rotating nature of RD wave in the canal appearing in the result of the rigorous method is produced by the secondary reflection of the wave which is nearly in a state of resonance (of lateral mode) for $kd=\pi$.

References

FILON, L. N. G., 1928. On a Quadrature Formula for Trigonometric Integrals, *Proc. Roy. Soc. Edin.*, **49**, 38-47.

MITSUI, H., 1967. Distribution of Wave Height in the Nearby Region of the Discontinuous Part of Coastal Structures (the second report) (in Japanese), *Collected Papers of the Fourteenth Coastal Engineering Conference in Japan*, 53-59.

MOMOI, T., 1965a, A Long Wave in the Vicinity of an Estuary [I]. *Bull. Earthq. Res. Inst.*, **43**, 291-316.

MOMOI, T., 1965b, A Long Wave in the Vicinity of an Estuary [II], *Bull. Earthq. Res. Inst.*, **43**, 459-498.

MOMOI, T., 1966, A Long Wave in the Vicinity of an Estuary [III], *Bull. Earthq. Res. Inst.*, **44**, 1009-1040.

MOMOI, T., 1967, A Long Wave around a Breakwater (Case of Perpendicular Incidence) [II], *Bull. Earthq. Res. Inst.*, **45**, 749-783.

MOMOI, T., 1968, A Long Wave in the Vicinity of an Estuary [IV], *Bull. Earthq. Res. Inst.*, **46**, 631-650.

STOKER, J. J., 1965, Water Waves, Pure and Applied Mathematics, Vol. IV, *Interscience Publishers, Inc., New York*, 109-147.

60. 河口近傍における長波について [V]

地震研究所　桃　井　高　夫

本報告においては河口近傍の合成波 (*resultant wave*), 反射回折波および河口水路への減衰モードが数値解析を通して論じられている. それによれば, 広海 (*open sea*) 領域において進入波の波高の 2 倍をこえる波高の領域および回転する波が現われている. この二つの現象は防波堤の風上側の水域 (垂直入射の場合) においても同様におきている. また水路への減衰波は水路のカベにそつて水路内に進み, 部分的に反射されて水路の中心軸にそつて広海にもどつている. 6 節においては河口近傍の波現象が直角隅角部のまわりの波現象と照合して論ぜられ, 更に 7 節においては直角隅角部のモデル二つを用いて鏡像の方法により河口近傍の長波が調べられている.